DTIC FILE COPY

(1)

SECURITY CLASSIFICATION OF THIS PAGE

AD-A217 908

REPORT DOCUMEN

Form Approved
OMB No. 0704-0188

1a. REPORT SECURITY CLASSIFICATION UNCLASSIFIED	1b. RESTRICTIVE MARKINGS NONE
2a. SECURITY CLASSIFICATION AUTHORITY	3. DISTRIBUTION/AVAILABILITY OF REPORT APPROVED FOR PUBLIC RELEASE; DISTRIBUTION UNLIMITED.
2b. DECLASSIFICATION/DOWNGRADING SCHEDULE	
4. PERFORMING ORGANIZATION REPORT NUMBER(S)	5. MONITORING ORGANIZATION REPORT NUMBER(S) AFIT/CI/CIA- 89-039
6a. NAME OF PERFORMING ORGANIZATION AFIT STUDENT AT UTAH STATE UNIVERSITY 6b. OFFICE SYMBOL (If applicable)	7a. NAME OF MONITORING ORGANIZATION AFIT/CIA
6c. ADDRESS (City, State, and ZIP Code)	7b. ADDRESS (City, State, and ZIP Code) Wright-Patterson AFB OH 45433-6583
8a. NAME OF FUNDING/SPONSORING ORGANIZATION 8b. OFFICE SYMBOL (If applicable)	9. PROCUREMENT INSTRUMENT IDENTIFICATION NUMBER
8c. ADDRESS (City, State, and ZIP Code)	10. SOURCE OF FUNDING NUMBERS PROGRAM ELEMENT NO. / PROJECT NO. / TASK NO / WORK UNIT ACCESSION NO.

11. TITLE (Include Security Classification) (UNCLASSIFIED)
Meteor Observations Using the 50 MHz Mentor Imaging Doppler Interferometer

12. PERSONAL AUTHOR(S)
Dennis Randall Thomas

13a. TYPE OF REPORT	13b. TIME COVERED	14. DATE OF REPORT (Year, Month, Day)	15. PAGE COUNT
THESIS/DISSERTATION	FROM _____ TO _____	1989	46

16. SUPPLEMENTARY NOTATION
APPROVED FOR PUBLIC RELEASE IAW AFR 190-1
ERNEST A. HAYGOOD, 1st Lt, USAF
Executive Officer, Civilian Institution Programs

17. COSATI CODES			18. SUBJECT TERMS (Continue on reverse if necessary and identify by block number)
FIELD	GROUP	SUB-GROUP	

19. ABSTRACT (Continue on reverse if necessary and identify by block number)

20. DISTRIBUTION/AVAILABILITY OF ABSTRACT ☒ UNCLASSIFIED/UNLIMITED ☐ SAME AS RPT. ☐ DTIC USERS	21. ABSTRACT SECURITY CLASSIFICATION UNCLASSIFIED
22a. NAME OF RESPONSIBLE INDIVIDUAL ERNEST A. HAYGOOD, 1st Lt, USAF	22b. TELEPHONE (Include Area Code) (513) 255-2259 22c. OFFICE SYMBOL AFIT/CI

DD Form 1473, JUN 86 — Previous editions are obsolete. — SECURITY CLASSIFICATION OF THIS PAGE

AFIT/CI "OVERPRINT"

Dennis Randall Thomas

METEOR OBSERVATIONS USING THE 50 MHZ MENTOR IMAGING DOPPLER INTERFEROMETER

Captain

United States Air Force

1989

52 Pages

Master of Science

Utah State University

ABSTRACT

Meteor Observations Using the 50 MHz MENTOR
Imaging Doppler Interferometer

by

Dennis Randall Thomas, Master of Science

Major Professor: Dr. Gene W. Adams
Department: Soil Science and Biometeorology

The MENTOR Imaging Doppler Interferometer radar operated at a frequency of approximately 50 MegaHertz with a 50 kilowatt peak power output. It was used to collect data from a field site near La Salle, Colorado on August 13, 1988. An algorithm was developed to detect meteor echoes in the Time Domain Averaged (TDA) data, separate these echoes from the rest of the data, and then determine which of these echoes were good enough to be included in wind calculations. The meteor detection rate for useable meteors in the approximately 9 minutes of data available in the study was 120 per hour. The meteors, after being located in three-dimensional space, were subjected to another algorithm which calculated the u, v, and w wind components for a range of altitudes, usually less than 4 kilometers, using the Doppler shift of the meteor echoes. Reasonable values for the wind components were obtained but could not be verified since there were no collateral data to back up the results.

(52 pages)

REFERENCES

Adams, G. W., D. P. Edwards, and J. W. Brosnahan, The imaging Doppler interferometer: Data analysis, Radio Sci., 20, 1481-1492, 1985.

Adams, G. W., J. W. Brosnahan, D. C. Walden, and S. F. Nerney, Mesospheric observations using a 2.66-MHz radar as an imaging Doppler interferometer: Description and first results, J. Geophys. Res., 91, 1671-1683, 1986.

Adams, G. W., Personal communications, 1988a.

Adams, G. W., Unpublished computer program, 1988b.

Aso, T., T. Tsuda, and S. Kato, Meteor radar observations at Kyoto University, J. Atmos. Terr. Phys., 41, 517-525, 1979.

Avery, S. K., A. C. Riddle, and B. B. Balsley, The Poker Flat, Alaska, MST radar as a meteor radar, Radio Sci., 18, 1021-1027, 1983.

Brosnahan, J. W., G. W. Adams, J. W. Neuschaefer, D. M. Woodard, and R. G. Roper, The MAPSTAR and MENTOR imaging Doppler interferometer radars, COSPAR Paper No. VI.1.6, 1988.

Davies, K., Ionospheric Radio Propagation, National Bureau of Standards Monograph 80, United States Department of Commerce, 1965.

Elford, W. G. and R. L. Craig, Upper atmosphere wind observations at Adelaide 35°S, August 1974, J. Atmos. Terr. Phys., 42, 61-67, 1980.

Forti, G., On the relation between diffusion coefficients and height from radar meteor echoes, J. Atmos. Terr. Phys., 40, 89-93, 1978.

Geller, M. A., S. A. Bowhill, and G. C. Hess, A description of the University of Illinois meteor radar system and some first results, J. Atmos. Terr. Phys., 39, 15-24, 1977.

Hess, G. C. and M. A. Geller, The Urbana Meteor radar system: Design, Development, and First Observations, Aeronomy report no.74, Aeronomy Lab, Dep. Elec. Eng., Univ. Ill., Urbana-Champaign, 1976.

Hey, J. S. and G. S. Stewart, Derivation of meteor stream radiants by radio reflexion methods, Nature, 158, 481-482, 1946.

Manning, L. A., O. G. Villard, Jr., and A. M. Peterson, Meteoric echo study of upper atmospheric winds, Proc. of the I.R.E., 38, 877-883, 1950.

McKinley, D. W. R., Meteor Science and Engineering, McGraw-Hill, Inc., New York, 1961.

Olsson-Steel, D. and W. G. Elford, The height distribution of radio meteors: observations at 2MHz, J. Atmos. Terr. Phys., 49, 243-258, 1987.

Pickard, G. W., A note on the relation of meteor showers and radio reception, Proc. of the I.R.E., 19, 1166-1170, 1931.

Roper, R. G., MWR-Meteor wind radars, MAP Handbook, 13, 124-134, November 1984.

Ruster, R., Winds and waves in the middle atmosphere as observed by ground-based radars, Adv. Space Res., 4, 3-18, 1984.

Schunk, R. W., The terrestrial ionosphere, in Solar-Terrestrial Physics, edited by R. L. Carovillano, and J. M. Forbes, pp.609-676, D. Reidel Publishing Company, New York, 1983.

Sugar, G. R., Radio propagation by reflection from meteor trails, Proc. of the IEEE, 52, 116-136, 1964.

Turek, R. S., An analysis of upper atmospheric parameters derived from the observation of meteor echoes by a 2.66 MHz radar, (Master's thesis), CASS Report GR-06, Utah State University, Logan, 1986.

METEOR OBSERVATIONS USING THE 50 MHZ MENTOR IMAGING DOPPLER INTERFEROMETER

by

Dennis Randall Thomas

A thesis submitted in partial fulfillment
of the requirements for the degree

of

MASTER OF SCIENCE

in

Soil Science and Biometeorology

(Aeronomy)

Approved:

Major Professor

Committee Member

Committee Member

Dean of Graduate Studies

UTAH STATE UNIVERSITY
Logan, Utah

1989

ACKNOWLEDGEMENTS

The material in this thesis is based upon work supported by the National Science Foundation under grants ATM-8608391, ATM-8719781, and ATM-8813454, the United States Air Force Office of Scientific Research under contract number F49620-89-C-022, and by a grant from Holodyne, Inc. I would also like to thank the United States Air Force for providing me the opportunity to attend Utah State University.

I would like to express my appreciation to Dr. Gene Adams who directed this research. Without his encouragement and assistance, this thesis would not have been possible.

I would also like to thank my Graduate Committee, Dr. Larry Hipps and Dr. Kent Miller, for their critical review of my thesis; Mr. John W. Brosnahan, Tycho Technology, Inc., Boulder, Colorado, for his tour of the facility where the MENTOR radar was constructed and of the radar site itself; Reese Johnson, for his expert advise on computer operations; and Teri Olsen, for her invaluable help in compiling this manuscript.

My greatest appreciation, however, is reserved for my wife, Cat, and my son, Jeremiah, who supported me through thick and thin. I was inspired by their unselfishness and all the love they showed to me throughout the many months of work. Without this support and love, this thesis would not have been completed.

Dennis Randall Thomas

TABLE OF CONTENTS

LIST OF TABLES

LIST OF FIGURES

ABSTRACT

Meteor Observations Using the 50 MHz MENTOR
Imaging Doppler Interferometer

by

Dennis Randall Thomas, Master of Science

Major Professor: Dr. Gene W. Adams
Department: Soil Science and Biometeorology

The MENTOR Imaging Doppler Interferometer radar operated at a frequency of approximately 50 MegaHertz with a 50 kilowatt peak power output. It was used to collect data from a field site near La Salle, Colorado on August 13, 1988. An algorithm was developed to detect meteor echoes in the Time Domain Averaged (TDA) data, separate these echoes from the rest of the data, and then determine which of these echoes were good enough to be included in wind calculations. The meteor detection rate for useable meteors in the approximately 9 minutes of data available in the study was 120 per hour. The meteors, after being located in three-dimensional space, were subjected to another algorithm which calculated the u, v, and w wind components for a range of altitudes, usually less than 4 kilometers, using the Doppler shift of the meteor echoes. Reasonable values for the wind components were obtained but could not be verified since there were no collateral data to back up the results.

(52 pages)

CHAPTER I

INTRODUCTION

Scientists are using a number of techniques to gain a better understanding of various processes in the Earth's atmosphere between 75 and 120 kilometers (km). These techniques include in-situ rocket soundings, observations from near-Earth satellites, various optical and acoustical methods, and ground-based radars. One of these techniques, radar, will be studied in detail to determine if it can provide enhanced measurement capabilities in this region of the atmosphere.

A powerful tool used in the study of the upper atmosphere is the ground-based radar. Ground-based radars are commonly used to measure atmospheric winds at heights above about 60 km. The meteor radar has been the most extensively used radar wind measurement technique to date. Pickard (1931) reported the earliest known incident of a radio effect resulting from the ablation of meteors in the upper atmosphere. He associated a general improvement in radio broadcast reception with meteor showers. However, little attention was actually given to the study of meteors until Hey and Stewart (1946) reported a clear correlation between radio signal variation and individual meteor trails. Computations of wind direction and velocity from radar observations of individual meteor trails were first attempted in the summer of 1949 by Manning et al. (1950). Over 300

papers on the radio properties of meteors appeared in the literature over the next ten years (Sugar, 1964).

Frictional heating and rapid ablation of meteoric particles, as well as columns of ionization, are produced as fast-moving meteoric particles collide with the neutral atmosphere. The ionized column is distributed in the form of a long, thin paraboloid with the particle at the head (Davies, 1965). Most meteor trails detected by current radar methods are observed between 80 and 120 km, with the highest frequency of occurrence observed between 92 and 95 km (Hess and Geller, 1976). Olsson-Steel and Elford (1987) suggest, however, that this value should be raised to 104 km based on their meteor study using a 1.98 MHz system. Above 120 km the atmosphere is too thin to cause ablation of meteors and below 80 km most meteors have completely evaporated due to the rapid change in atmospheric density which occurs over this height range. These meteor trails can become tracers of neutral air motions since they are embedded in the atmosphere at heights where high ion-neutral collision frequencies exist, approximately 3×10^5/s. Most meteor wind radars in use today operate at frequencies between 30 and 50 MegaHertz (MHz). These radars measure the Doppler shift of signals that are specularly reflected from the meteor trails. To obtain the meridional (north-south) and zonal (east-west) components of the wind, two antenna beams, looking at right angles to each other, are normally formed. The vertical

component of the wind is considered to be negligible for these calculations.

After the meteor trail forms, the ions and electrons expand radially in an electrically neutral cloud under the influence of ambipolar diffusion. Some meteor radars can, therefore, determine the rate of ambipolar diffusion in the atmosphere by measuring the change in the received power at the antenna. By calculating the ambipolar diffusion coefficients, the atmospheric diffusion scale height and the atmospheric density at these levels may be deduced (Ruster, 1984). Turek (1986) provides a detailed description of how ambipolar diffusion coefficients can be determined using meteor data.

The temporal resolution of the meteor-derived wind measurements is dependent on two factors; the rate of meteor echoes observed and the adopted averaging interval. The spatial resolution, on the other hand, depends only on the specific operating parameters of the individual radar system. Typical resolution values for meteor wind radars are about 30 to 60 minutes (temporal) and 4 km (spatial). Many of these meteor radar systems do not have a height-ranging capability, therefore, wind values are assigned to an altitude in the mid-range of the meteor zone, usually about 95 km (Ruster, 1984).

The system used to collect data for this study operated at a frequency of 50 MHz, which is consistent with several

other meteor radar systems. At this frequency a great deal of information can be obtained from meteor echoes using conventional meteor radars. The unique aspect of the MENTOR system is its use of Imaging Doppler Interferometry (IDI) techniques to determine the meteor's position in three-dimensional space. Because the MENTOR Imaging Doppler Interferometer radar is unique, several data processing algorithms must be developed from scratch.

Objectives

The specific objectives of this research are:

1) Develop an algorithm to detect meteors using the 50 MHz MENTOR Imaging Doppler Interferometer.
2) Develop an algorithm to describe meteor trail locations in an X, Y, and Z coordinate system where X is east, Y is north, and Z is the altitude.
3) Develop an algorithm to determine the east-west (u), north-south (v), and vertical (w) components of the neutral wind.

CHAPTER II

LITERATURE REVIEW

Meteoric particles travel in elliptical orbits around the sun and may be divided into three classes; micro-meteorites, meteorites, and meteors. Micrometeorites are extremely small particles that settle through the atmosphere without being completely burned up by frictional heating (ablated). Though a large number of micrometeorites enter the atmosphere, they are of little concern in radar studies, since, by the time they reach an altitude where they can be studied by meteor radars, they are moving so slowly that they interact little with the atmospheric constituents and, therefore, are not detectable by radar methods. On the other hand, meteorites or extremely large meteoroids that actually reach the Earth's surface produce significant ionization, but their rate of occurrence is extremely low, making them difficult to study. Meteors, those particles entering the Earth's atmosphere that are completely ablated, produce a significant amount of ionization in the atmosphere and have a high rate of occurrence. This makes meteors a primary concern in radar studies (Sugar, 1964).

Meteors are generally divided into two types. The first type is shower meteors which are defined as collections of associated particles all moving with the same velocity in fairly well-defined orbits around the sun. Their orbits

intersect the Earth's orbit around the sun at a specific time each year producing meteor showers. Even though shower meteors often produce spectacular visual effects and are often photographed, they account for only a very small portion of the meteors observed by radar.

The second type, sporadic meteors, is of primary concern in this study. The orbits of these meteors are not associated with each other but seem to move randomly around the sun. While the radiants and times of occurrence of sporadic meteors appear to be random, they seem to be concentrated toward the ecliptic plane and they move in the same direction around the sun as the Earth. Their orbits are not distributed uniformly along the Earth's orbit but are concentrated so as to produce an annual cycle in the meteor detection rate. The maximum influx of meteors usually occurs during July-September and the minimum usually occurs during February-March (McKinley, 1961; Avery et al., 1983). The occurrence rate of sporadic meteors is also influenced by the motion of the Earth as it revolves. This results in a regular diurnal variation in the meteor rate. On the morning side of the Earth, the forward motion effectively "sweeps up" meteoric particles, but on the evening side the only meteors reaching the Earth are those which overtake it, resulting in a maximum meteor occurrence rate at around 0600 Local Time (LT) and a minimum occurrence rate at around 1800 LT.

A summary of some of the estimated properties of different sporadic meteoric particles is shown in Table 1. The particles of interest to most meteor radar systems range in mass from 10^{-6} to 10^{-2} grams (Olsson-Steel and Elford, 1987). The velocities of meteors approaching the Earth range between 11.3 and 72 km/s. The minimum velocity, relative to the Earth, is the escape velocity for a particle leaving the Earth and is, therefore, the lowest velocity that a particle falling toward the earth can have. The maximum velocity is the sum of two components, a 30 km/s component associated with the velocity of the Earth in its orbit around the sun, and a 42 km/s component associated with the meteor itself as it travels through the solar system (Sugar, 1964).

The height distribution of observable meteor trails varies with the meteor's velocity, mass, and radiant. According to McKinley (1961), the radiant is the point where the meteor path intersects the celestial sphere, or the point at infinity on the meteor path, assuming a linear extension backward of the visible line segment. In simpler terms, the radiant is the spot in the sky from which the meteor appears to have come.

Meteors with a high velocity and/or large zenith angle produce trails at higher altitudes than those of lower velocity and/or smaller zenith angle. Meteors with high mass produce a lower maximum ionization height. For most current meteor radars, the maximum number of returns is observed at

TABLE 1. Order-of-Magnitude Estimates of the Properties of Sporadic Meteors (adopted from Sugar, 1964).

PARTICLE TYPE	MASS (g)	RADIUS	NUMBER/DAY
MICROMETEORITES	10^{-12} 10^{-11} 10^{-10} 10^{-9}	0.4 μm 0.8 μm 2 μm 4 μm	10^{20}
METEORS	10^{-8} 10^{-7} 10^{-6} 10^{-5} 10^{-4} 10^{-3} 10^{-2} 10^{-1} 1 10 10^{2} 10^{3}	8 μm 20 μm 40 μm 80 μm 0.02 cm 0.04 cm 0.08 cm 0.2 cm 0.4 cm 0.8 cm 2 cm 4 cm	? 10^{12} 10^{11} 10^{10} 10^{9} 10^{8} 10^{7} 10^{6} 10^{5} 10^{4} 10^{3} 10^{2}
METEORITES	10^{4}	5 - 8 cm	10

around 92 km (Hess and Geller, 1976). Olsson-Steel and Elford (1987) suggest, however, that this value should be raised to 104 km based on their meteor study using a 1.98 MHz system. This system, which operated only at night to avoid interference from the E-layer, allowed them to raise the ceiling on detectable meteors to 140 km and, thus, evaluate many more meteors than most meteor radars.

Meteor trails can be divided into two types according to their radio reflection properties. The first type is the underdense trail where the electron density produced is low enough to allow the incident radio wave to penetrate the trail. The trail can then be considered to be a group of individual scattering electrons, however, the scattering due to the individual electrons is not observed. What is observed is the collective backscattering due to all the electrons in the meteor trail as determined by the orientation of the trail in space.

The second type is the overdense trail where the density of electrons is high enough to cause secondary scattering from electron to electron to become important. The electrons no longer act as independent scatterers, and the incident wave does not penetrate the column. This results in the total reflection of the radio wave (Sugar, 1964).

According to Sugar (1964), underdense trails are the predominant type seen by meteor radars. Since the reflection from the trail is specular, only those trails

which are perpendicular to the radar beam are detected. The received-to-transmitted power ratio is given by:

$$P_R/P_T = G_T G_R \lambda^3 q^2 r_e^2 / 32\pi^2 R^3 \exp(-8\pi^2 r_o^2/\lambda^2) \exp(-32\pi^2 D_a t/\lambda^2) \qquad (2.1)$$

where

P_T = the transmitted power

P_R = the received power

G_T = the power gain of the transmitting antenna relative to an isotropic radiator in free space

G_R = the power gain of the receiving antenna relative to an isotropic radiator in free space

λ = the radar wavelength

R = distance from the radar to the trail

r_e = classical radius of the electron (2.8178×10^{-15} m)

q = electron line density of the trail (number of electrons per unit length)

r_o = initial radius of the meteor trail (which has been measured to be between 0.55 and 4.35 m)

D_a = ambipolar diffusion coefficient which can be given as $D_a = r^2/4t$ where r is the effective radius of the trail (Sugar, 1964) or, according to Schunk (1983), $D_a = kT/m\upsilon$ where k is Boltzmann's constant, T is the temperature, m is the mass, and υ is the collision frequency

t = time, measured from formation of the trail which is assumed to be instantaneous.

After the meteor has produced a trail of effective radius r_o, the main factor in reducing the echo strength is ambipolar diffusion. As diffusion causes the charged particles produced by the meteor to expand radially, destructive interference within the trail occurs, producing an underdense trail and reducing the echo amplitude. In the underdense meteor trail, the power received falls off exponentially as a function of the ambipolar diffusion coefficient, D_a. This produces an echo amplitude decay time or decay time constant T_d given by:

$$T_d = \lambda^2/16\pi^2 D_a \qquad (2.2)$$

and is defined as the time taken for the echo amplitude to decrease by a factor of e, or the time for the received power to decrease by a factor of e^2. T_d is dependent on the radar wavelength, λ, and D_a which depends on density and altitude.

Equation (2.1) shows the power received from the meteor return varies as λ^3, while Equation (2.2) shows the echo duration time varies as λ^2. This suggests that the longer the radio wavelength, the better the radar system for meteor research. However, at wavelengths greater than 10 m, interference from distant stations due to ionospheric reflections can occur, particularly in daylight hours during sunspot maxima. In addition, wavelengths greater than 20 m can be seriously affected by daytime absorption effects below the normal E region and by reflection from the E region. These two factors put an effective cap on the upper

wavelength limit. Therefore, most contemporary radio meteor systems operate at frequencies above 30 MHz to avoid reflection and absorption from the ionosphere. Observations at these high frequencies, however, are normally limited to meteor trails below about 100 to 110 km, since higher echoes become too weak to detect. The theoretical echo height "ceiling" increases from approximately 105 to 125 km as the radar wavelength is increased from 6 m (50 MHz) to 100 m (3 MHz). Lower frequencies can raise the height of this ceiling if the observations are taken when the E region electron densities are sufficiently low (McKinley, 1961). In fact, Olsson-Steel and Elford (1987) suggest a ceiling of 140 km at 1.98 MHz. In addition, the duration of the echoes is much longer at these wavelengths, allowing easier study of the echo characteristics.

To determine the variation with height and time of the wind field in the meteor region, the following parameters of each echo must be determined:

1. The radial velocity of the drifting trail;
2. The echo range;
3. The echo arrival (zenith) angles; and
4. The echo occurrence time (Roper, 1984).

The radial velocity can be determined from the Doppler shift of the received signal. The echo range may be determined by a suitable range-gating scheme. The two most common techniques used to determine the echo arrival angle involve

relative amplitude measurements (McKinley, 1961) and interferometry (Aso et al., 1979). The relative amplitude method involves comparison of echo amplitudes from two different antennas which have different patterns in the vertical plane. These antenna patterns vary with the echo arrival angle, therefore, comparing the two amplitudes will give the echo arrival angle.

Interferometry involves the comparison of phase differences between the signals received at two or more spatial locations to locate a target (Adams et al., 1986).

In addition to neutral wind measurements, meteor radars can also be used to infer the atmospheric mass density and the appropriate diffusion scale height (H). This is done by matching an exponential curve to the echo decay data and then determining the ambipolar diffusion coefficient, D_a, using Equation (2.2). The diffusion scale height (H) can then be inferred from the value of D_a. This can be done using the following linear equation, assuming an isothermal atmosphere:

$$H = (h-C)/\ln(D_a) \qquad (2.3)$$

where h is the altitude in km and C is a constant (Forti, 1978; Turek, 1986). The atmospheric density can then be inferred from the scale height using the relation

$$n = n_o \exp[-(h-h_o)/H] \qquad (2.4)$$

where n_o represents the density at some reference altitude (h_o) (Schunk, 1983).

CHAPTER III

DATA ANALYSIS

The MENTOR Imaging Doppler Interferometer Radar

The data used in this analysis of meteor echoes were recorded by the MENTOR Imaging Doppler Interferometer (IDI) radar which is located at 104°35'55"W, 40°16'42"N, east of La Salle, Colorado. MENTOR, an acronym which stands for Meteor Echoes; No Transmitter, Only Receivers, was initially designed as a passive system, receiving pulses reflected out of Stratospheric-Tropospheric (ST) radar beams by meteor trails. Later, a 50 kilowatt transmitter was added so a stand-alone IDI radar, suitable for tropospheric and stratospheric studies as well as meteor measurements, now exists.

Radar echoes are received on 8 independent antennas and sampled at 40 range gates for Time Domain Averaged (TDA) data. The software supports 256-point complex Fast Fourier Transforms (FFT) on the data streams. The data from each channel are separately Fourier-transformed and the resulting complex Fourier spectra at each range gate are examined for Doppler bins whose sources can be located by antenna-to-antenna phase differences (spatial interferometry). Real atmospheric sources are identified by requiring agreement among the several independent antenna pairs on the two-dimensional angular location of each source. When combined

with the time-of-flight (range gate) information, this gives a three-dimensional location of each scattering point.

The MENTOR system operates at approximately 50 MHz (49.8 or 49.92 MHz) with a 50 kilowatt peak-pulse-power and a pulse length of 1.67 or 6.67 microseconds (μs). The system uses two identical arrays of 16 five-element Yagi antennas, one as a transmitter and one as a receiver (Fig. 1).

The transmit antennas are directed vertically and arrayed in a four-by-four matrix with 1.05-0.7-1.05 wavelength spacing between both the row and column antennas. A 16-way power splitter feeds the antennas with equal power and phase resulting in a beam approximately 20° wide at the 3 decibel (dB) points.

Each receive antenna contains a preamplifier for noise-figure establishment and the 16 signals are recombined with 4-way power combiners to obtain a total of 8 outputs consisting of 4 row arrays and 4 column arrays. Each antenna has a somewhat fan-shaped pattern 20° wide at the 3 dB points in the narrow dimension (along the line of Yagis), but about 50° wide perpendicular to the line of Yagis (Brosnahan et al., 1988).

Complex voltages are recorded in-phase, the x component, as well as with a 90° phase shift or in-quadrature, the y component. The x and y components can then be used to determine the phase and power of the received signal (Adams et al., 1985):

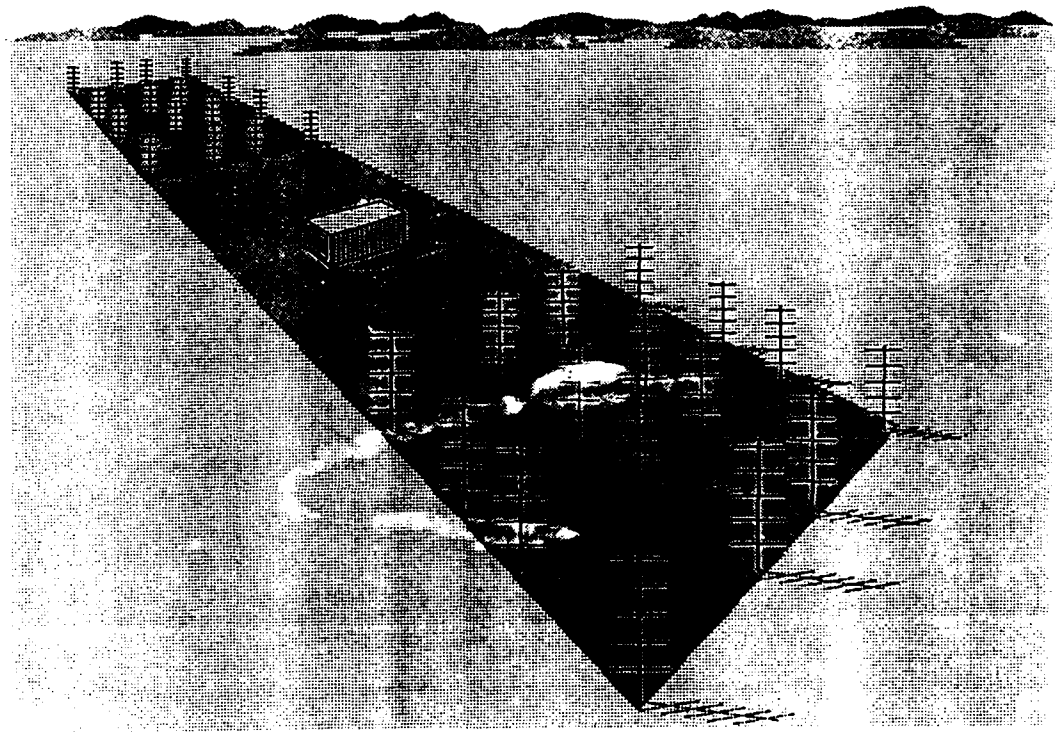

Fig. 1. Antenna array configuration for the MENTOR Imaging Doppler Interferometer (IDI) radar.

$$\text{phase} = \tan^{-1}(y/x) \quad (3.1)$$

$$\text{power} = x^2 + y^2 \quad (3.2)$$

The MENTOR system uses a direct-conversion receiver technique. Eight channels are used to amplify and detect the eight antenna signals. Two Bessel filters are available for each quadrature channel allowing the operator to select between two bandwidths. Each complete sounding with 256 samples takes 10 seconds. The TDA data are written to magnetic tape allowing the operator to check the functioning of the system and do specific TDA calculations such as: identifying meteors, deriving winds, and deriving densities from the returns; calculating spaced-antenna-drift winds for comparison with the meteor winds and with the Mesospheric-Stratospheric-Tropospheric (MST) radar and IDI radar winds; and tracking Traveling Ionospheric Disturbances (TIDs) (Brosnahan et al., 1988).

The data analyzed for this study were recorded from 1954 Universal Time (UT) or 1354 Local Time (LT), August 13, 1988, to 2003 UT or 1403 LT, August 13, 1988. A total of 53 data files were processed through the meteor detection and analysis algorithms.

A total of 40 range gates were sampled for each of the 8 antennas. A range gate spacing of 1 km was selected with a bottom range (range 1) of 80 km and a top range (range 40), therefore, corresponding to 120 km (Adams, 1988a).

Imaging Doppler Interferometry

The Imaging Doppler Interferometry (IDI) technique uses returns from a radar pulse, range gating, several independent antenna-receiver-processor channels, Doppler frequency sorting, and spatial interferometry to characterize clear-air and partial-reflection scattering in terms of the three-dimensional location, Doppler velocity, and scattering amplitude and phase of each discrete scattering center (Brosnahan et al., 1988). If two or more dipole antennas are connected, a spacing of length d between the two antennas gives the relation between the phase difference (ϕ) and the zenith angle (θ) of the target as:

$$\phi = 2\pi/\lambda = (2\pi d \sin\theta)/\lambda \qquad (3.3)$$

The IDI method uses the measured phase differences across the north-south and east-west antenna arrays to locate targets. Time series of recorded complex voltages from each antenna in the array are first Fourier-transformed. Since a complex Fourier transform returns both an amplitude and a phase at each Doppler frequency, individual spectral features can be located from the phase differences between antennas. The phases are those of each spectral component at time t = 0. Even though the data have been Fourier-transformed, the phase information has been preserved.

To demonstrate a one-dimensional case, consider a single target moving at some horizontal velocity (V_h) above a two-antenna interferometer. The Fourier-transformed power

spectra for the two antennas identify the same Doppler frequency (f). This frequency can then be used to calculate the target's radial velocity (V_R) using the following equation:

$$V_R = fc/2F = V_h \sin\theta \qquad (3.4)$$

where c is the speed of light and F is the radar frequency. The phase difference at the target's Doppler frequency can be used in Equation (3.3) to calculate the target's zenith angle.

If we include range-gating and extend this technique to two orthogonally spaced antenna arrays, the necessary information to determine a target's position in three-dimensional space is available. Using multiple targets at *different* altitudes, this technique can generate a three-dimensional image of the atmosphere, thus the name Imaging Doppler Interferometer (Adams et al., 1986).

To determine the zenith angles in both the east-west and north-south planes, the following process is used. First, three independent phase differences, one from the 0.7λ pair (antennas two and three) and the other two from the 1.05λ pairs (antennas one and two and antennas three and four), are calculated. Each phase difference corresponds to one or more possible zenith angles through the interferometer equation:

$$\text{Phase Difference} = -2\pi d \cdot \sin(ZA) \qquad (3.5)$$

where ZA is the zenith angle and d is the antenna spacing in wavelengths. There are three independent measures of the

east-west zenith angle which will spread across some range of zenith angles and, simultaneously, three independent measures of the north-south zenith angle and their resultant spread. This requires the sum of the two zenith angle spreads in each direction derived from the three independent phase differences, the 0.7λ pair and the two 1.05λ pairs, be less than the zenith angle window for one of the possible ± 2π permutations. The zenith angle window for the meteor detection algorithm is set at 51°. This simultaneously filters out most of the random points and resolves the ambiguity in the zenith angle. The two cardinal zenith angles which result from this process are called the consensus angles since they represent agreement between the three values. The final zenith angle is determined by maximizing a "rule-of-thumb" measure of the accuracy:

$$\text{Accuracy} = (Ni)^{\frac{1}{2}} \cdot (Nc) \cdot d \qquad (3.6)$$

where Ni is the number of incoherent operations, Nc is the number of coherent operations, and d is the antenna spacing. Antennas one and two, phase shifted and coherently summed, are used as one antenna of the final interferometer, and antennas three and four are used as the other antenna. Since the general location of the echo is already known, the ambiguity is easy to deal with.

The spacing for the final pair is 1.75λ, for which there are five possible solutions for the zenith angle from a single phase difference. All that needs to be done now is

pick the value (if any) that lies within one half of the zenith angle window centered around the concensus. If the final value lies outside of this value, it is rejected. Next, calculate the five possible zenith angles until you find a match. If a match is not found the point is rejected.

Since θ_{ew} and θ_{ns} are determined independently, there are combinations that do not represent possible locations in a real three-dimensional world. For example, it is impossible to be on the eastern and northern horizons simultaneously. If no real altitude is possible the point must be rejected.

After identifying a good point, "steer" the full array toward the point and determine its power and phase. Instead of actually steering the antenna beam, this really translates the point into the zenith. The phase reference is now the geometric middle of the array. Each direction is steered and the voltage amplitudes and phases are determined separately (Adams, 1988b).

Information available for each identifiable scattering point now consists of:

the radial velocity (V_R);

the range gate (R), in 1 km steps;

the zenith angle in the east-west plane (θ_{ew}); and

the zenith angle in the north-south plane (θ_{ns}).

The range and the two zenith angles form a three-dimensional coordinate system which is then transformed into a Cartesian coordinate system where X is east, Y is north, and Z is the

altitude. The parameters for each scattering point are then sorted by altitude. Since the location of each scattering point has been determined and the scalar value of the radial velocity can be determined using equation (3.4), the vector radial velocity is given by

$$\mathbf{V}_{Rj} = V_{Rj}\mathbf{1}_{Rj} \tag{3.7}$$

where j = 1, 2, 3,..., n, where n is the number of scattering points at a particular altitude, and $\mathbf{1}_{Rj}$ is a unit vector in the radial direction passing through the jth point, and is given by

$$\mathbf{1}_{Rj} = l_j\mathbf{1}_x + m_j\mathbf{1}_y + n_j\mathbf{1}_z \tag{3.8}$$

where l_j, m_j, and n_j are the direction cosines of the jth scattering point, given by

$$l = \sin(\theta_{ew}) \tag{3.9}$$

$$m = \sin(\theta_{ns}) \tag{3.10}$$

$$n = (1 - l^2 - m^2)^{\frac{1}{2}} \tag{3.11}$$

The mean apparent-motion vector for each altitude can be given by

$$\mathbf{V}_m = u\mathbf{1}_x + v\mathbf{1}_y + w\mathbf{1}_z \tag{3.12}$$

where u, v, and w correspond to the east-west, north-south, and vertical wind components, respectively. With at least three scattering points the three components of the motion can be determined with the following three equations:

$$u\Sigma(l_j)^2 + v\Sigma l_j m_j + w\Sigma l_j n_j = \Sigma V_{Rj} l_j \tag{3.13}$$

$$u\Sigma l_j m_j + v\Sigma(m_j)^2 + w\Sigma m_j n_j = \Sigma V_{Rj} m_j \tag{3.14}$$

$$u\Sigma l_j n_j + v\Sigma m_j n_j + w\Sigma(n_j)^2 = \Sigma V_{Rj} n_j \tag{3.15}$$

where $V_{Rj} = V_m \cdot 1_{Rj}$. This gives three equations with three unknowns which can easily be solved (Adams et al., 1986).

Meteor Detection

The data analysis to determine meteor trail drift and, therefore, the character of the upper atmospheric winds is similar to the IDI method. However the meteor data are subjected to time-domain interferometry techniques rather than being Fourier-transformed before analysis because the meteor echo is assumed to have a single distinct Doppler frequency. Additional adjacent frequencies given by a fast Fourier transform would adversely affect the resulting wind calculations. Therefore, the meteor trail data are removed from the raw data and analyzed separately before any other calculations.

This introduces the problem of recognizing the meteor echoes when they appear in the data. This can be done qualitatively by visual inspection of the data. Figure 2 shows a plot of signal amplitude versus time. The large, rapid increase in amplitude can be identified as a meteor echo. Distinct phase patterns also exist for these echoes in both the east-west (Fig. 3) and north-south (Fig. 4) directions. Even though visual inspection of the data can lead to the detection of meteors, an automated selection procedure needed to be devised.

For each raw data file in this study an average power for the east-west and north-south antenna arrays are

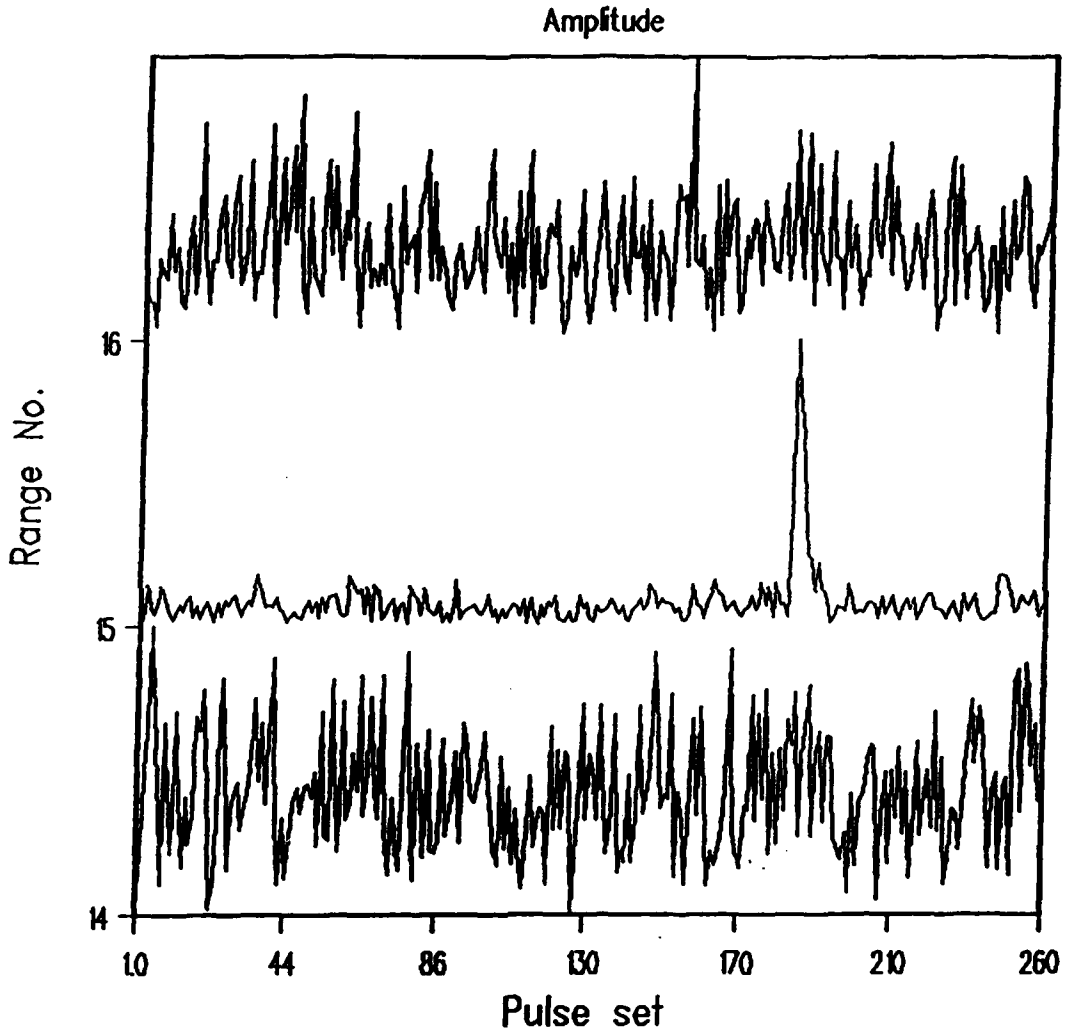

Fig. 2. Meteor echo in the Time Domain Averaged data (2000 UT, August 13, 1988).

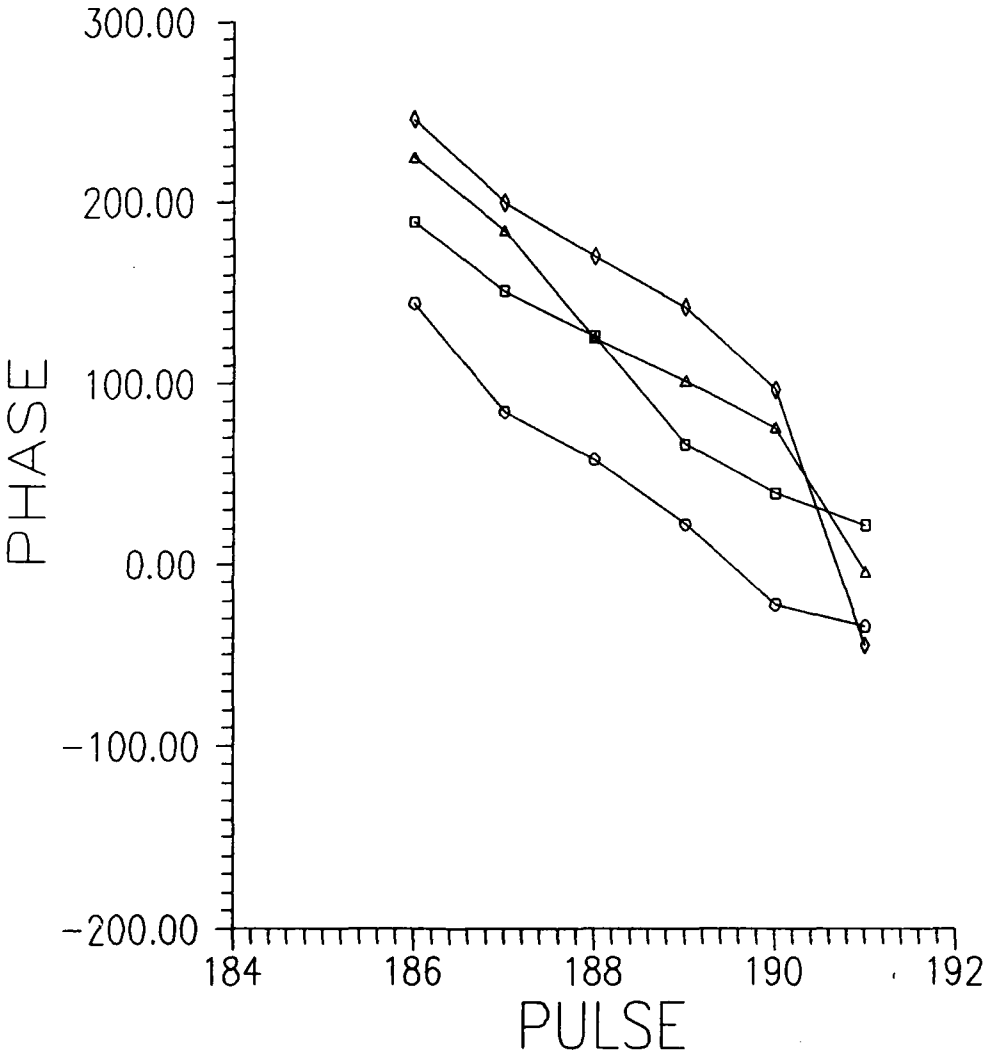

Fig. 3. Plot of the phase values for each antenna in the east-west direction (2000 UT, August 13, 1988).

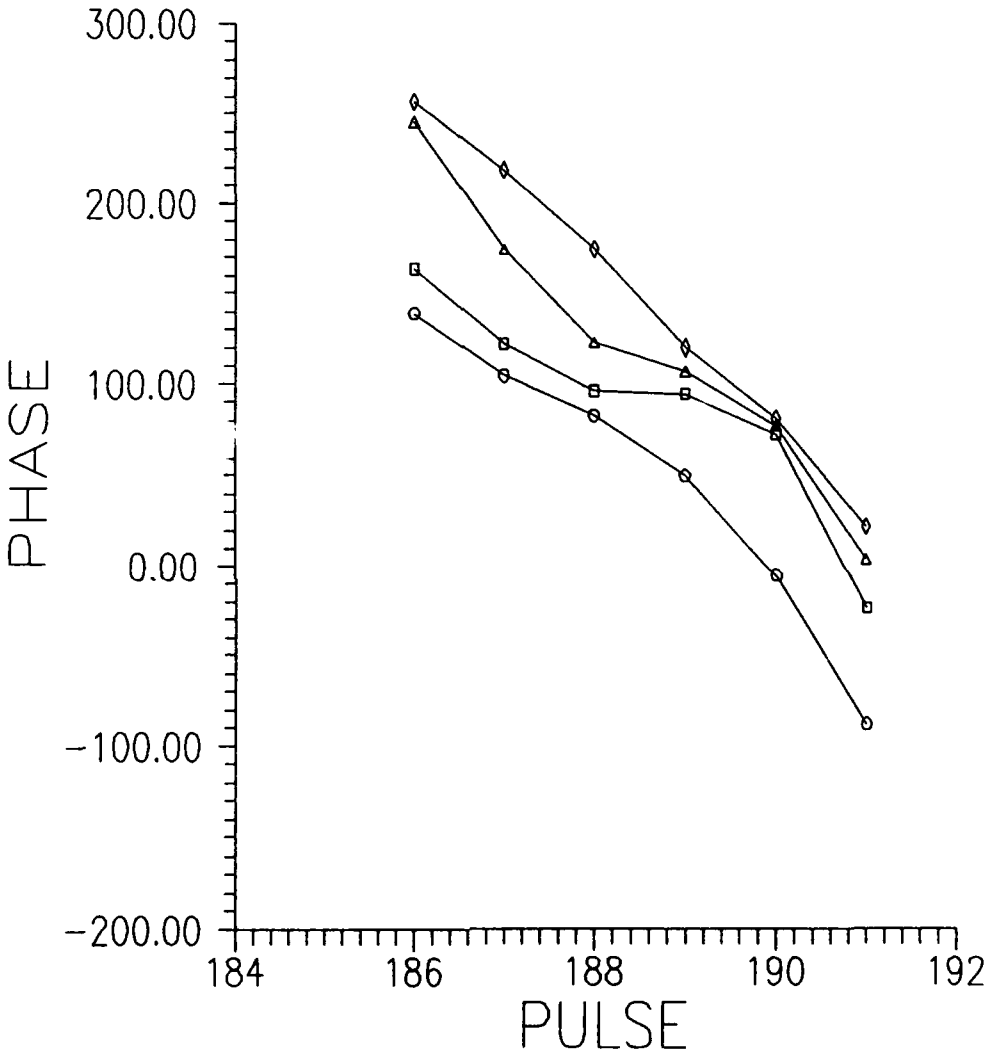

Fig. 4. Plot of the phase values for each antenna in the north-south direction (2000 UT, August 13, 1988).

calculated for each range by coherently summing the complex voltages for each pulse and dividing by 256. If the power for an individual pulse is greater than 3 dB above this average power, then the point is removed and the power is averaged again over the remaining points, thus giving an average "noise" level.

Next, it is necessary to locate large increases in the power amplitude over the average noise level. This jump in power amplitude results from an ionization column produced as the meteor collides with the neutral atmosphere. The meteor detection algorithm looks for returns that satisfy certain minimum requirements. Echoes that remain 5 dB or more above the average noise for at least four consecutive pulses are considered to be returns of a "real" target and, therefore, need further analysis.

Once a valid target is found, the pulse representing the peak power must be identified. This peak power pulse contains information relative to the speed of the meteor and would, therefore, contaminate any computed wind values. Thus, only those pulses after this peak power pulse are used in the analysis (Turek, 1986). The meteor detection algorithm introduces another filter at this point. There must be at least two pulses above the average noise following the peak power pulse or the echo is rejected. The justification for this filter lies in the calculation of the Doppler frequency which will be discussed shortly.

Phase values for each antenna are then calculated for each of the pulses within the echo using equation (3.1). These phase values are then corrected for any 2π discontinuities which may exist (Adams et al., 1985). The two zenith angles, θ_{ew} and θ_{ns}, are then calculated just as in the IDI method.

Since the meteor echo data are not first Fourier transformed, another method for determining the Doppler frequency must be used. The Doppler frequency in the time domain can be obtained by finding the time derivative of the phase, $d\phi/dt$. This, of course, requires at least two points be present in the data. The Doppler frequency, f, for the nth pulse is approximated by

$$f(n) = [\phi(n) - \phi(n-1)]/\Delta t \qquad (3.16)$$

where Δt is the time between pulses. Since the phase of the nth pulse is also used to calculate the Doppler frequency for the nth+1 pulse, only those phase differences corresponding to every other pulse within the meteor are used. The radial velocity can then be calculated using equation (3.4).

Since the radar does not give sufficient spatial resolution to accurately locate each point on the meteor trail, the radial velocity for both the east-west and north-south directions for each pulse within a given meteor echo are averaged to give a single representative value for each. A comparison of these averaged radial velocities is then made. The echo is accepted only if the averaged radial

velocity is positive for both directions or negative for both directions. This eliminates ambiguous values resulting from one being positive and the other being negative. For those echoes which survive, the radial velocities for the two directions are then averaged to give a single representative value for the meteor echo.

The θ_{ew} and θ_{ns} values for each pulse within the meteor echo are also averaged to give a single representative value for each. Using these averaged values, the X, Y, and Z coordinates of the echo are determined by

$$X = R\sin(\theta_{ew}) \tag{3.17}$$

$$Y = R\sin(\theta_{ns}) \tag{3.18}$$

$$Z = R\cos(RZA) \tag{3.19}$$

where R is the range and RZA, the radial zenith angle in radians, is given by

$$RZA = \sin^{-1}(\sin^2\theta_{ew} + \sin^2\theta_{ns})^{\frac{1}{2}} \tag{3.20}$$

Close to zenith, a small error in the calculated radial velocity can result in large errors in the resulting horizontal motion (Adams et al., 1986). Therefore, a filter which eliminates those points which are less than 5° from zenith is imposed at this point in the algorithm. Also, since each antenna's pattern is somewhat fan-shaped and only 20° wide at the 3 dB points (Brosnahan et al., 1988), those points which are outside of 20° are eliminated.

Using only those meteor echoes which survived all of the imposed filters, the u, v, and w wind components are then

calculated in the same way as the IDI method. One difference is that the resulting winds are not for a specific altitude but for a range of altitudes. This is because at least three points (echoes in this case) are needed to reach a solution using equations (3.9) to (3.11) and (3.13) to (3.15). With all of the filtering processes which take place in the algorithm, it is unlikely that three meteors at the same altitude will survive during such a short period of operation.

CHAPTER IV

RESULTS AND DISCUSSION

Meteor Echo Detection

For the 53 data files analyzed in this study a total of 140 echoes, some of which were the same meteor at different ranges, were detected using the meteor detection algorithm. By the time these echoes were processed through the various filters mentioned in Chapter III, only 18 were considered good enough to include in the wind analysis algorithm. None of these surviving echoes showed up on more than one range so these were separate and distinct meteors. Since there are only about 9 minutes of data present, this corresponds to a detection rate of 120 'good' meteors per hour.

The meteor detection rate of the MENTOR Imaging Doppler Interferometer radar is quite favorable when compared with the rates from both MST radars that have been operated as meteor radars and conventional meteor radar systems. For example, from 1980 to 1981 the 50 MHz MST radar located at Poker Flat, Alaska, when operating as a meteor radar with a peak power of 400 kilowatts, had an effective meteor detection rate of four per hour (Avery et al., 1983). Conventional meteor radars which operate from 27 to 50 MHz and peak powers of less than 100 kilowatts average meteor echo detection rates from 10 to 50 per hour (Geller et al., 1977; Elford and Craig, 1980). Turek (1986) reported a

detection rate of 58 per hour using the 2.66 MHz IMAGER radar with its 50 kilowatt peak power located at the Boot Lake field site near Brighton, Colorado. The highest reported meteor detection rate, approximately 300 per hour, is from the meteor radar system operated by the University of Illinois-Urbana. This radar has a very high powered transmitter with a peak power of 5 megawatts and an antenna which is specifically designed for meteor detection (Hess and Geller, 1976).

The detection rates just mentioned have been averaged over at least a 24 hour period for all of these radar systems except the IMAGER radar system studied by Turek (1986). The test data from the MENTOR radar only represents the period from 1354 to 1403 local time. Since meteor activity is normally higher in the morning hours and lower in the evening hours, the detection rate could be expected to be slightly higher than 120 per hour when averaged over a 24 hour period. This slight increase could, however be offset by a change in season since the maximum influx of meteors occurs in the July to September time frame (McKinley, 1961; Avery et al., 1983).

After a 'good' meteor is located, its radial velocity, θ_{ew}, θ_{ns}, radial zenith angle, X coordinate, Y coordinate, and Z coordinate (altitude), are determined using the methods described in the previous chapter.

Figure 5 shows a plot of meteor locations relative to the position of the receivers using the calculated zenith

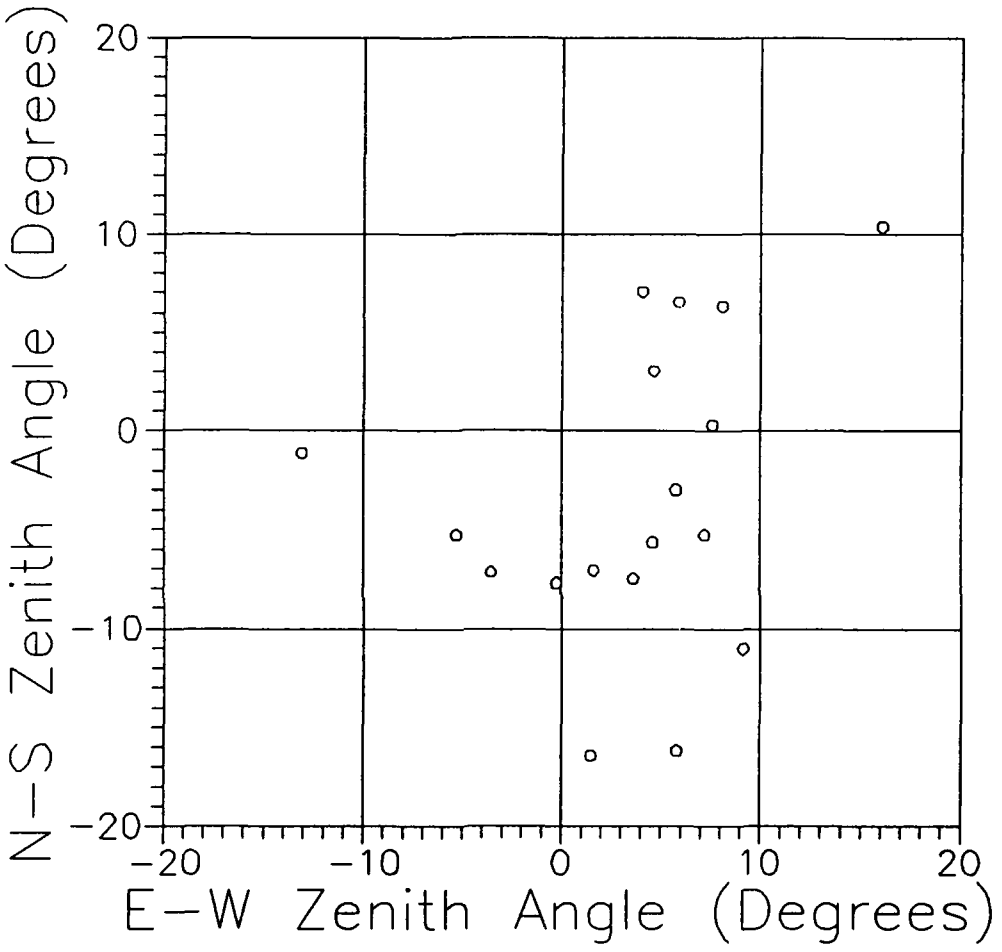

Fig. 5. Zenith angle location grid for each 'good' meteor within the study.

angles in the east-west and north-south planes. The receivers' positions are the point on the graph designated 0.00-0.00. The meteor echo locations show little correlation with each other except that they are concentrated more to the east and south of the receivers.

Since the radial zenith angle is required to be between 5 and 20 degrees after filtering of the meteor echoes and the minimum range is set at 80 km, the lowest altitude for which a meteor can actually be detected is 75 km and the highest altitude is 119.5 km. The lowest meteor in the study was detected at 78.8 km and the highest was at 116.5 km. The majority of meteors, however, were found below 111 km. Between the 78 and 111 km region, there was no altitude which dominated the height distribution of the echoes, however, there was a noticeable lack of meteors between 94 and 101 km. Table 2 shows the altitudes of each of the meteor echoes and how the meteors were grouped to determine the u, v, and w wind components. The average altitude for each grouping is also given and is used as a reference altitude for the other graphs in this section. Since the highest meteor, 116.5 km, was not close to the other groups of meteors, it was omitted from the wind calculations.

Wind Analysis

After the meteors were split into groups of three or more, the u, v, and w wind components could be determined using the method described in Chapter III. Table 3 shows the

TABLE 2. Altitudes of Each 'Good' Meteor and Average Altitudes for Each Range of Altitudes in Each Group.

Altitude (km)	Average Altitude for Each Group (km)
78.8	
81.7	80.8
81.8	
84.5	
84.8	85.0
85.7	
90.6	
91.5	
93.5	92.3
93.7	
101.2	
101.3	
105.7	103.5
105.8	
109.0	
110.3	110.0
110.7	
116.5	Not Used

TABLE 3. Three Component Wind Speeds and Horizontal Wind Directions for the Meteor Wind Analysis Technique.

Average Altitude (km)	U (m/s)	V (m/s)	W (m/s)	Horizontal Wind Direction
80.8	37.8	-15.3	3.4	112.0°
85.0	68.4	-13.0	-6.0	100.8°
92.3	85.7	-96.8	-1.5	138.5°
103.5	-83.8	36.1	14.9	293.3°
110.0	-28.4	44.7	3.6	327.6°

results of the wind calculations for each altitude range. Figures 6, 7, and 8 show a graphical representation of this same information broken down by the east-west (u), north-south (v), and vertical (w) components, respectively. The horizontal wind direction was also calculated and is represented in Figure 9. The wind direction given here is the direction the wind is moving. For example, a wind direction of 135° means the wind is moving towards the southeast.

Even though some of the values seem to be relatively large compared to values in the lower atmosphere, they are, considering the altitudes, quite reasonable. It should be realized that these calculated values have certain inherent errors associated with them. For instance, the zenith angle accuracy in degrees is ± (zenith angle window/15). Since a value of 51° was chosen for the zenith angle window in the meteor detection algorithm, the accuracy for the zenith angle values is ± 3.4°. This can introduce a sizeable error in the resulting wind calculations.

In addition to zenith angle errors, there are also errors in phase. The phase accuracy in degrees is ± [zenith angle window · (11/15)]. This corresponds to a possible error of 37.4 degrees in the phase measurements. This could introduce a significant error into the phase differences used to calculate the Doppler frequency and, therefore, the radial velocity. This can alter the resulting wind calculations

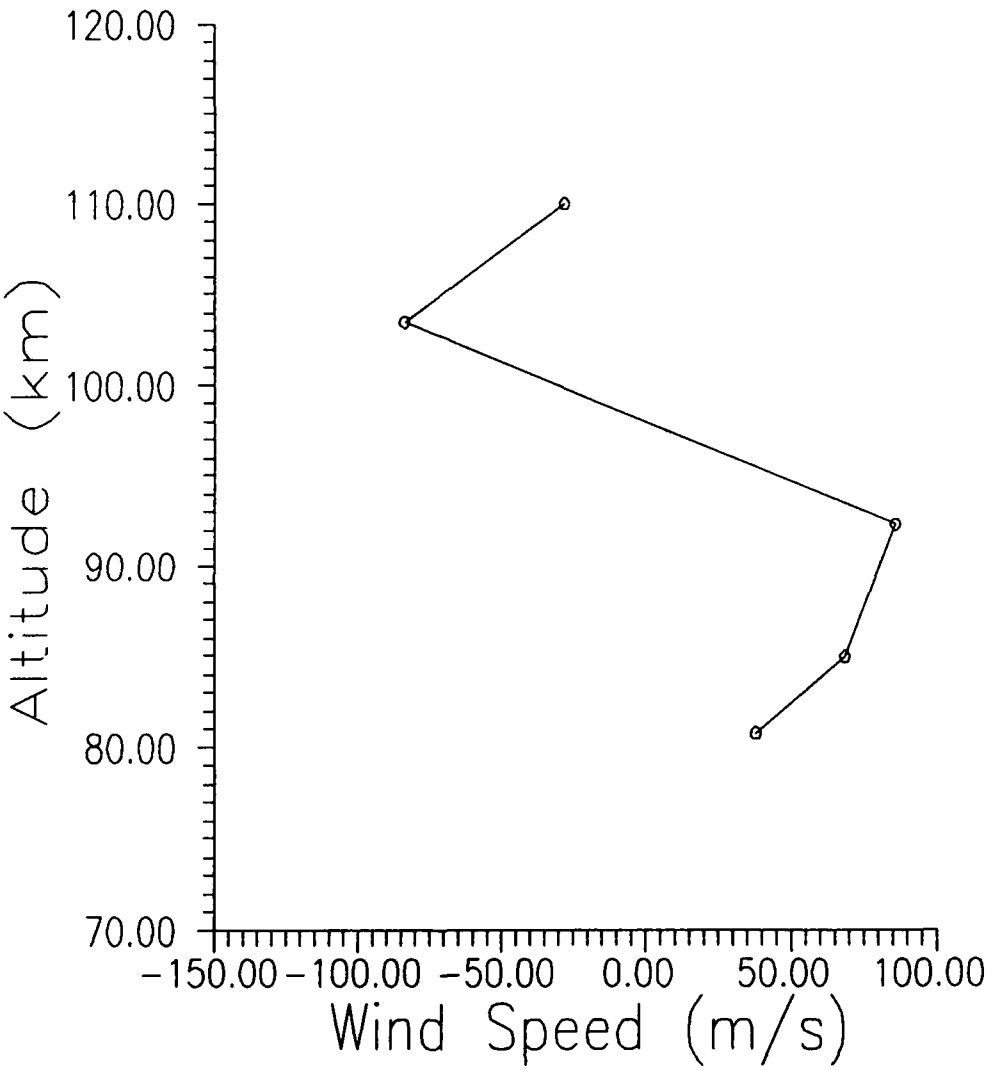

Fig. 6. Plot of the east-west wind component, u, at each averaged altitude representing an altitude range.

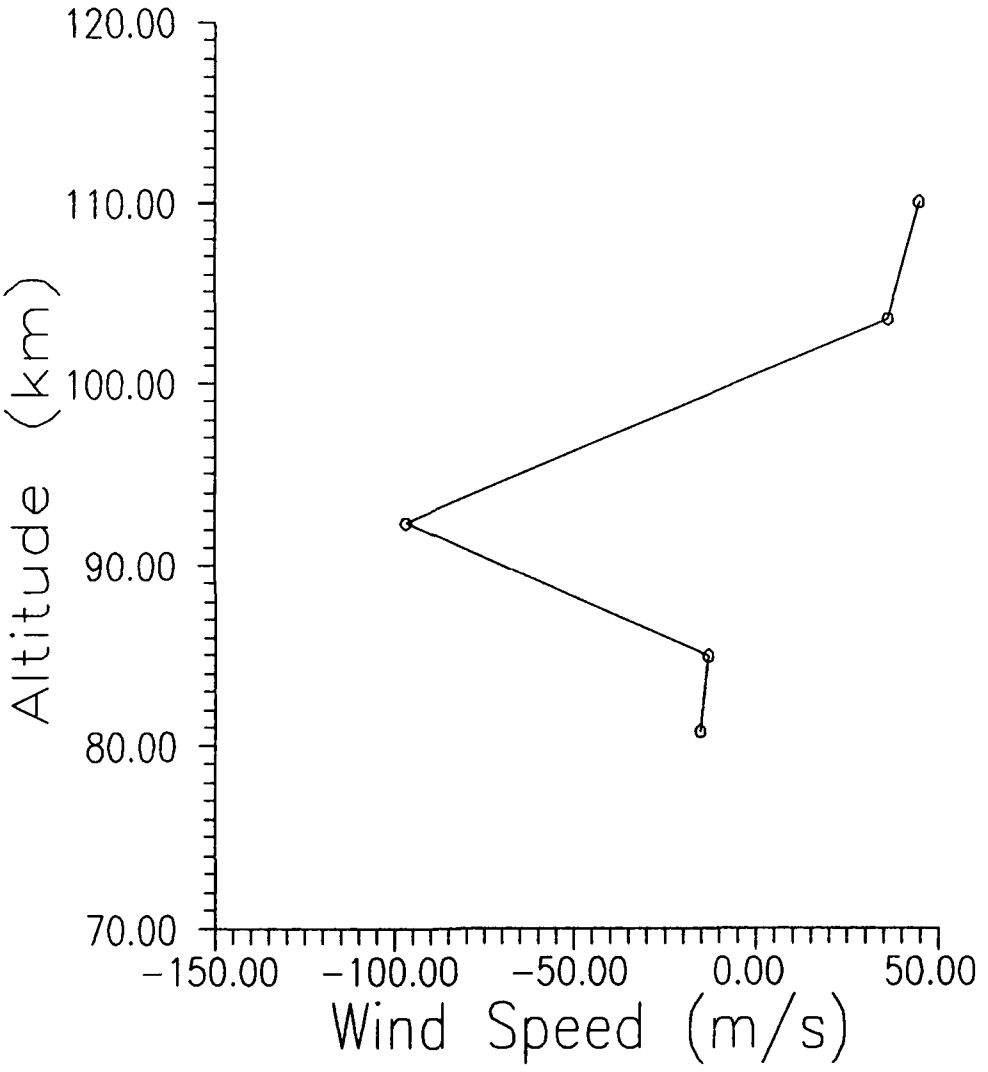

Fig. 7. Plot of the north-south wind component, v, at each averaged altitude representing an altitude range.

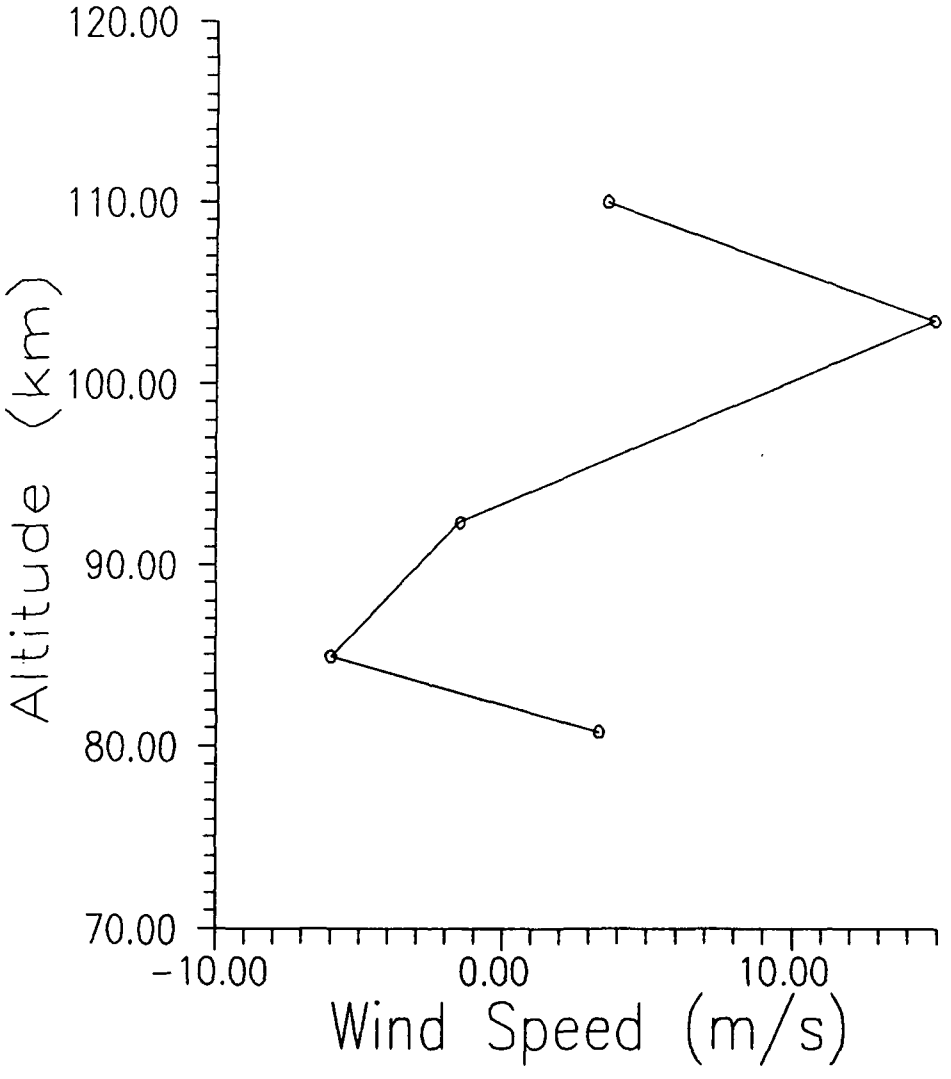

Fig. 8. Plot of the vertical wind component, w, at each averaged altitude representing an altitude range.

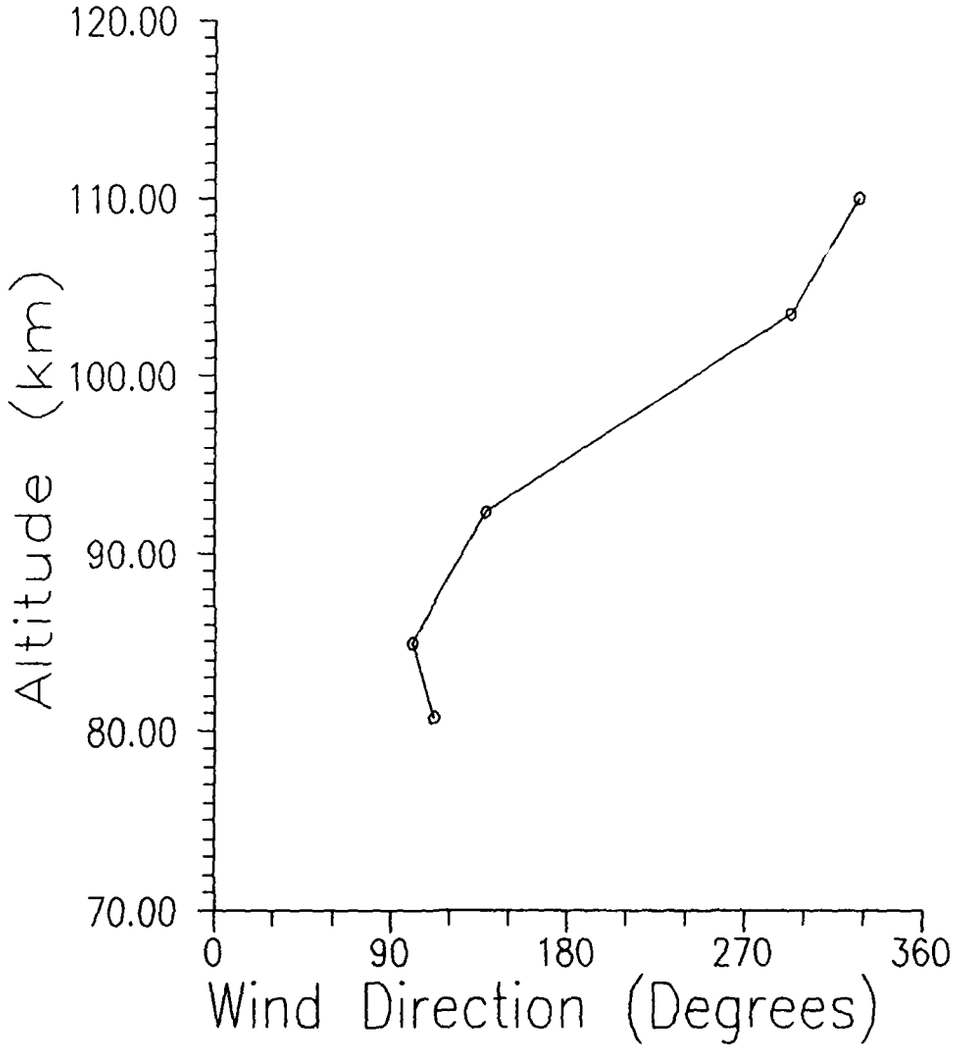

Fig. 9. Plot of the horizontal wind direction at each averaged altitude representing an altitude range.

considerably.

The horizontal wind values can vary as much as 34 percent in this algorithm. For instance, a value of 50 m/s could be as low as 33 m/s and as high as 67 m/s (Adams, 1988b).

Without collateral data to back up the findings, it is difficult to know whether or not the algorithms need any modifications. If any modifications are needed they should only be slight adjustments to some of the restrictive numerical values introduced in the program such as the zenith angle window, the 3 dB limit for determining which points to remove in the average noise calculation, the 5 dB limit for determining which echoes are 'good', the number of consecutive pulses required for 'good' echoes, and the relative agreement between the velocities from the east-west and north-south antennas.

CHAPTER V

CONCLUSIONS

Algorithms were developed to locate meteors in the 50 MHz MENTOR Imaging Doppler Interferometer radar data, locate these meteors in an x, y, and z, coordinate system, and determine the u, v, and w components of the neutral wind at meteor altitudes. The data were first processed through the meteor detection algorithm to locate as many meteor echoes as possible. These echoes were then removed from the remainder of the data and passed through a series of filters to determine which echoes could be used in subsequent calculations. Out of 140 echoes detected originally, only 18 survived the filtering process producing a detection rate for 'good' meteors of 120 per hour. This detection rate is considerably higher than detection rates for most conventional meteor radars with similar peak power outputs and optimized detection algorithms (Elford and Craig, 1980; Geller et al., 1977) and for the IMAGER IDI radar described by Turek (1986). Following the selection of 'good' meteor echoes, they were put in groups of three or more so the u, v, and w wind components could be calculated. The resulting values seemed reasonable but, without collateral data, are impossible to validate.

Recommendations for Further Research

With less than 10 minutes of data present for analysis,

it is difficult to determine how a particular system will perform over long periods of time. It would be beneficial to operate this system continuously for an extended period of time to see if it still performs as well as it did for this short test. Without any collateral data to support the results, the algorithms cannot be fine tuned to produce wind calculations with the smallest possible errors. Any extended campaign should, out of necessity, be coordinated with other wind detection campaigns so the validity of the results can be checked.

REFERENCES

Adams, G. W., D. P. Edwards, and J. W. Brosnahan, The imaging Doppler interferometer: Data analysis, Radio Sci., 20, 1481-1492, 1985.

Adams, G. W., J. W. Brosnahan, D. C. Walden, and S. F. Nerney, Mesospheric observations using a 2.66-MHz radar as an imaging Doppler interferometer: Description and first results, J. Geophys. Res., 91, 1671-1683, 1986.

Adams, G. W., Personal communications, 1988a.

Adams, G. W., Unpublished computer program, 1988b.

Aso, T., T. Tsuda, and S. Kato, Meteor radar observations at Kyoto University, J. Atmos. Terr. Phys., 41, 517-525, 1979.

Avery, S. K., A. C. Riddle, and B. B. Balsley, The Poker Flat, Alaska, MST radar as a meteor radar, Radio Sci., 18, 1021-1027, 1983.

Brosnahan, J. W., G. W. Adams, J. W. Neuschaefer, D. M. Woodard, and R. G. Roper, The MAPSTAR and MENTOR imaging Doppler interferometer radars, COSPAR Paper No. VI.1.6, 1988.

Davies, K., Ionospheric Radio Propagation, National Bureau of Standards Monograph 80, United States Department of Commerce, 1965.

Elford, W. G. and R. L. Craig, Upper atmosphere wind observations at Adelaide 35°S, August 1974, J. Atmos. Terr. Phys., 42, 61-67, 1980.

Forti, G., On the relation between diffusion coefficients and height from radar meteor echoes, J. Atmos. Terr. Phys., 40, 89-93, 1978.

Geller, M. A., S. A. Bowhill, and G. C. Hess, A description of the University of Illinois meteor radar system and some first results, J. Atmos. Terr. Phys., 39, 15-24, 1977.

Hess, G. C. and M. A. Geller, The Urbana Meteor radar system: Design, Development, and First Observations, Aeronomy report no.74, Aeronomy Lab, Dep. Elec. Eng., Univ. Ill., Urbana-Champaign, 1976.